

Distribution Agreement

In presenting this thesis as a partial fulfillment of the requirements for a degree from Emory University, I hereby grant to Emory University and its agents the non-exclusive license to archive, make accessible, and display my thesis in whole or in part in all forms of media, now or hereafter now, including display on the World Wide Web. I understand that I may select some access restrictions as part of the online submission of this thesis. I retain all ownership rights to the copyright of the thesis. I also retain the right to use in future works (such as articles or books) all or part of this thesis.

Caroline Spancake

March 30, 2023

Development of a Targeted Identification Platform of Small Molecule Inhibitors for Rare and Orphan Diseases

by

Caroline Spancake

Christina Gavegnano
Adviser

Chemistry

Christina Gavegnano
Adviser

Dennis Liotta
Committee Member

Eric Miller
Committee Member

2023

Development of a Targeted Identification Platform of Small Molecule Inhibitors for Rare and Orphan Diseases

By

Caroline Spancake

Christina Gavegnano

Adviser

An abstract of
a thesis submitted to the Faculty of Emory College of Arts and Sciences
of Emory University in partial fulfillment
of the requirements of the degree of
Bachelor of Science with Honors

Chemistry

2023

Abstract

Development of a Targeted Identification Platform of Small Molecule Inhibitors for Rare and Orphan Diseases

By Caroline Spancake

Rare and orphan diseases are often under-researched due to their limited financial incentive to pharmaceutical companies. Drug repurposing provides a unique, beneficial approach which reduces costs, leverages small patient populations, limited resources, and lowers other barriers in rare and orphan disease drug discovery and development. This project aimed to establish and optimize a screening platform and workflow for rare and orphan diseases by evaluating therapeutic agents for their ability to serve as treatments or reversals of phenotypes. Multisystem Proteinopathy 1 (MSP-1) was the model disease for this development, with a therapeutic approach to employ candidates aiming to reverse phenotypes driven by harmful levels of protein aggregation. Candidates were screened for efficacy, toxicity, impact on various diseases markers, and reversal of phenotypes that drive disease *in vivo*. Future directions include pursuit of advanced efficacy platforms and expanding the scope of the project to other diseases or full classes of diseases, with a streamlined goal of selection of repurposed agents to expedite the path to the clinic with a robust, informed preclinical package.

This thesis is private and is not a public disclosure.

Development of a Targeted Identification Platform of Small Molecule Inhibitors for Rare and Orphan Diseases

By

Caroline Spancake

Christina Gavegnano

Adviser

A thesis submitted to the Faculty of Emory College of Arts and Sciences
of Emory University in partial fulfillment
of the requirements of the degree of
Bachelor of Science with Honors

Chemistry

2023

Acknowledgements

A very special thank you to Dr. Gavegnano for giving me the opportunity to pursue and develop a project which means so much to me. I have learned so much in a short period of time, and I am extremely appreciative of all that you've done for me. Your guidance and support have been invaluable to the project, and I am beyond excited to see how this project continues to progress and evolve. I would also like to thank everyone in the Gavegnano lab- thank you for your help, support, and sense of camaraderie this past year. A special thank you to Emily for all that you do for the lab and listening to my random thoughts and ideas throughout the way.

I also want to thank everyone in the Raj lab (special shoutout to Victor, Angele, Ashish, Ben, and Rachel) for helping me navigate research as a new undergrad, learn, and grow as a chemist.

To my committee members- Dr. Liotta and Dr. Miller, thank you for serving on my committee, I am grateful for your time and guidance.

Finally, I could not do any of this without the love and patience of my friends and family. Thank you for believing in me every step of the way.

Table of Contents

Introduction	3
Background.....	5
<i>Disease History</i>	<i>5</i>
<i>Clinical Manifestations</i>	<i>7</i>
<i>Role of VCP/p97 in MSP1</i>	<i>8</i>
<i>VCP Function in Protein Clearance</i>	<i>10</i>
<i>Relationship between Autophagy and the Ubiquitin Proteasome System</i>	<i>11</i>
<i>Therapeutic Approach</i>	<i>12</i>
Methods	14
<i>Initial Cell Culture</i>	<i>14</i>
<i>MTS Assay</i>	<i>18</i>
<i>Reactive Oxidative Species (ROS) Detection & Optimization</i>	<i>19</i>
<i>Autophagy Assay</i>	<i>19</i>
Results	20
<i>Toxicity Screening</i>	<i>20</i>
<i>ROS Detection</i>	<i>27</i>
<i>Autophagy Studies</i>	<i>22</i>
Discussion & Future Direction.....	33
<i>Toxicity Studies.....</i>	<i>33</i>
<i>ROS Detection</i>	<i>34</i>
<i>Autophagy Studies</i>	<i>33</i>
<i>Rare and Orphan Disease Drug Discovery.....</i>	<i>35</i>
References	37

Table of Figures

Figure 1- Drug discovery timeline and benefits to drug repurposing.....	2
Figure 2- Visualization of therapeutic index.....	3
Figure 3- Time of MSP-1 identification and classification.....	4
Figure 4- Valosin Containing Protein (VCP) structure (PDB: 5FTK (A,B) 7RL6 (C)).....	6
Figure 5- VCP regulates protein degradation pathways which are targeted to reduce or reverse phenotypic outcomes.....	11
Figure 6- 5,000 Cells per well initially established as optimal.....	14
Figure 7- Optimization of cellular plating density of freshly thawed cells.....	15
Figure 8- Summary of compound cytotoxicity assessed by MTS tetrazolium-based uptake assay.....	17
Figure 9- Compounds of interest do not inhibit cell growth asses by MTS Assay.....	18
Figure 10- Effect on rufinamide on autophagy and apoptosis markers of activation and autophagosome induction in HIV-1 vector transduced primary human monocyte derived macrophages.....	19
Figure 11- Compounds of interest reduce autophagic vacuole accumulation.....	21
Figure 12- Autophagy assay staining visualization.....	23
Figure 13- Additional staining conducted in growth media for improved visualization.....	24
Figure 14- Preliminary data suggests inhibition of Reactive Oxygen Species (ROS) production in dysregulated MSP cells.....	25
Figure 15- Optimization of ROS Assay- Effects on Phosphate buffered Saline (DPBS) Rinse on ROS Detection.....	26
Figure 16- Compounds of interest inhibit production of ROS.....	27
Figure 17- Nuclear staining as an internal control for ROS Assay.....	29
Figure 18- Workflow for rare and orphan drug discovery.....	32

Introduction

Rare diseases are defined as any disease that affects less than 200,000 people in the United States, with the National Institute of Health (NIH) identifying over 7,000 rare diseases. Approximately 1 in every 10 Americans suffers from a rare disease and this impact is estimated to affect at least 350 million people worldwide.¹ Despite this expansive burden, over 95% of rare diseases still lack approved treatments, underscoring a major unmet clinical need for individuals suffering from these diseases.¹ While orphan diseases are considered rare diseases, orphan diseases receive a distinct label to denote neglect in research and drug development. Orphan drugs are defined by the 1984 US Orphan Drug Act to be a treatment for diseases affecting fewer than 200,000 people *or* not being profitable for at least seven years.² Due to small populations of individuals suffering from these diseases, there is a small market space which lacks financial incentive to pharmaceutical companies. In addition to a lack of pharmaceutical interest and cost barriers, these small populations pose additional challenges in many aspects as there is limited existing literature, difficulties in conducting clinical trials, and other barriers to achieving regulatory approval. While there has been worldwide policy efforts to promote the development of orphan medical products (OMPs), there is still a lack of innovative research and development as 72% of development is still focusing on rare disease areas that already have existing treatments.³ As such, there is a significant unmet clinical need. Academic drug discovery, specifically drug repurposing, poses a unique and beneficial approach to rare and orphan drug discovery, facilitating an informed approach that can reduce time and cost as demonstrated in Figure 1.

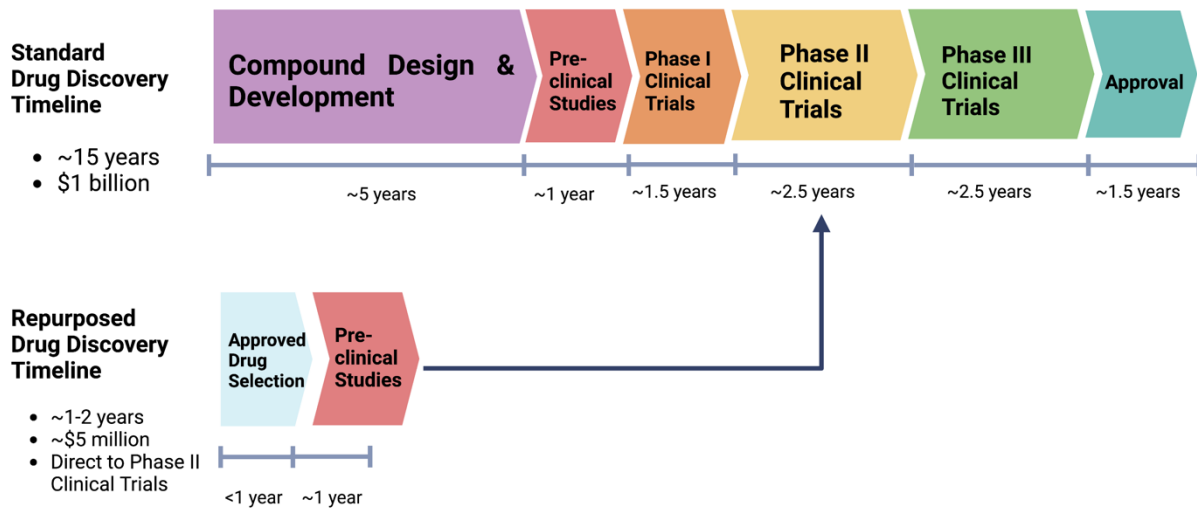


Figure 2- Drug discovery timeline and benefits to drug repurposing

Barriers that are unique to rare and orphan diseases such as limited patient populations for clinical trials, access to biologically relevant resources, and pharmaceutical incentive are partially ameliorated with drug repurposing. With already established, robust and approved data such as safety, pharmacokinetics, including drug-drug interactions, pharmacological mechanisms across routes of administration, metabolism, distribution, and excretion, the path to clinical efficacy evaluation is expedited.⁴ Additionally, in disease models in which the pathophysiology is unknown or yet to be fully elucidated, employing agents with known mechanism of action can aid in developing a better understanding of diseased states. As such, this works seeks to develop a platform for rare and orphan disease drug discovery in academic setting by identifying novel, safe agents in a high throughput manner for an expedited path to the clinic.

Background

Drug discovery is a complex and time intensive process, beginning with the identification of diseased states or targets of interest. Rare and orphan diseases require a unique approach as many diseases have unknown or deemed “undruggable” targets, thus the project began with an approach to disease selection centered around creation of a screening platform with key readouts focused on reversal of disease phenotype with evaluated candidate agents. Determination of potential drug candidate’s toxicity and efficacy profile is a critical in early stages of drug discovery to establish a therapeutic index as demonstrated in Figure 2, and is central to drug repurposing.⁵ As such, *in vitro* toxicity and

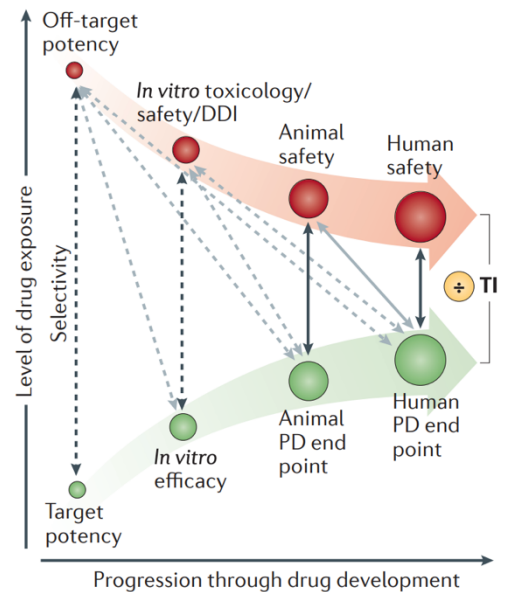


Figure 3- Visualization of therapeutic index

Adapted from Nat. Rev. Drug Discov. 2012

efficacy screening and optimization in diseased cellular models was considered a central aim of this platform development. In order to maintain a rare disease perspective, Inclusion Body Myopathy with Early onset Paget’s Disease/Multisystem Proteinopathy-1 was chosen as the model disease.

Disease History

Inclusion Body Myopathy with Early onset Paget’s Disease and Frontotemporal Dementia (IBMPFD) now referred to as Multisystem Proteinopathy 1 (MSP1) is an inherited pleiotropic disorder that can affect muscle, bone, and the nervous system.⁶ The disorder dates back to 1966 as a single case of Paget’s disease of bone (PDB) with an autosomal dominant pattern of inheritance

and later in 1982 as a similarly inherited case of PDB with motor neuron disease. In the early 2000s early onset PDB was associated with the limb girdle muscular dystrophy, illuminating a similar pattern in cases of concurrent inclusion body myopathy, PBD, and frontotemporal dementia and was determined to be a genetically unique and distinct disorder.⁷ Mutations in the VCP gene (also referred to as p97) were identified as the pathogenic cause and the syndrome was named IBMPFD and considered a VCP disease. However, this name did not stand the test of time as other phenotypic markers became associated with the disorder and other genes were quickly identified to be causative in patients without VCP mutations.⁸ Pathogenic mutations in hnRNPA1 and hnRNPA2b1 occurred in families with identical phenotypes as IBMPFD, yet did not have VCP mutations.⁹ As such, there was a 2013 movement to change the name of the syndrome to Multisystem Proteinopathy (MSP), conferring inclusivity of various phenotypes, and specifically MSP-1 for VCP-mutation driven cases, with other genetic markers receiving specific nomenclature. While this nomenclature has since been encouraged and reinforced by experts in the field, the variety in names over time poses a unique challenge in MSP research. Many of the already limited cell lines, existing literature, and other resources utilize the outdated name of IBMPFD causing confusion and obstacles to further progress in drug discovery and disease understanding.

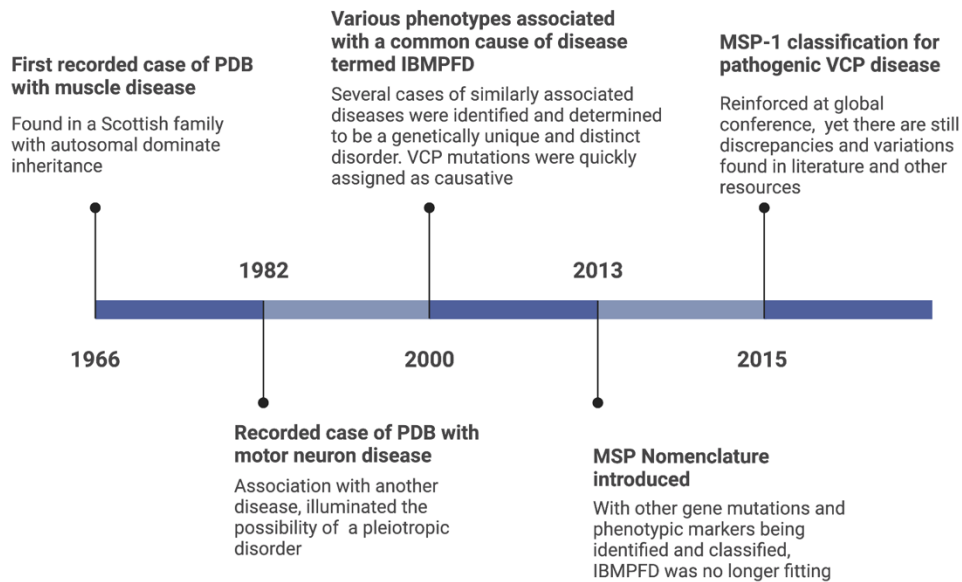


Figure 4- Timeline of MSP-1 identification and classification

Clinical Manifestations

MSP1 is an autosomal dominant disorder leading characterized by one or more phenotypes of Inclusion Body Myopathy (IBM, ~90% of individuals), Paget disease of bone (PDB, ~50%), and Frontotemporal dementia (FTD, ~30%).⁷ While less common, the disease has also presented associated manifestations of Parkinson disease (PD), amyotrophic lateral sclerosis (ALS), and other diseases. Muscle weakness due to myopathy often leads to loss of mobility, wheelchair dependency, and difficulties in day-to-day functions. PDB can cause bone pain, deafness, nerve compression and other bone related complications. Individuals suffering from FTD or other neurological diseases suffer from reduced cognitive function, behavioral impairment, and other debilitating neurological symptoms.¹⁰ This pleiotropic disorder is complex and causes a significant decrease in quality of life, with death usually due to respiratory failure due to weakening in cardiac muscles.¹¹ A current standard of care was recently developed and focuses on phenotype

specific approaches based off diseases with similar phenotypes as there is a lack of evidence and understanding to the disease. There are currently no approved disease modifying therapies. Early detection through genetic testing and multidisciplinary care teams are vital in current supportive care. ¹⁰

Role of VCP/p97 in MSP1

MSP1 is caused by mutations encoding valosin-containing protein (VCP) also referred to as p97, with over 50 heterozygous missense mutations in *VCP* associated with MSP1. VCP is a hexameric protein containing stacked ATPase domains (D1 and D2) connected via linkers and a N-domain on the outskirts as shown in Figure 1. ¹² Most pathogenic mutations occur between the N- and D1- domains, which suggest possible interactions between these regions in diseased states. The specific cell line utilized in this work contains a mutations at the R155H position as shown in Figure 1C.

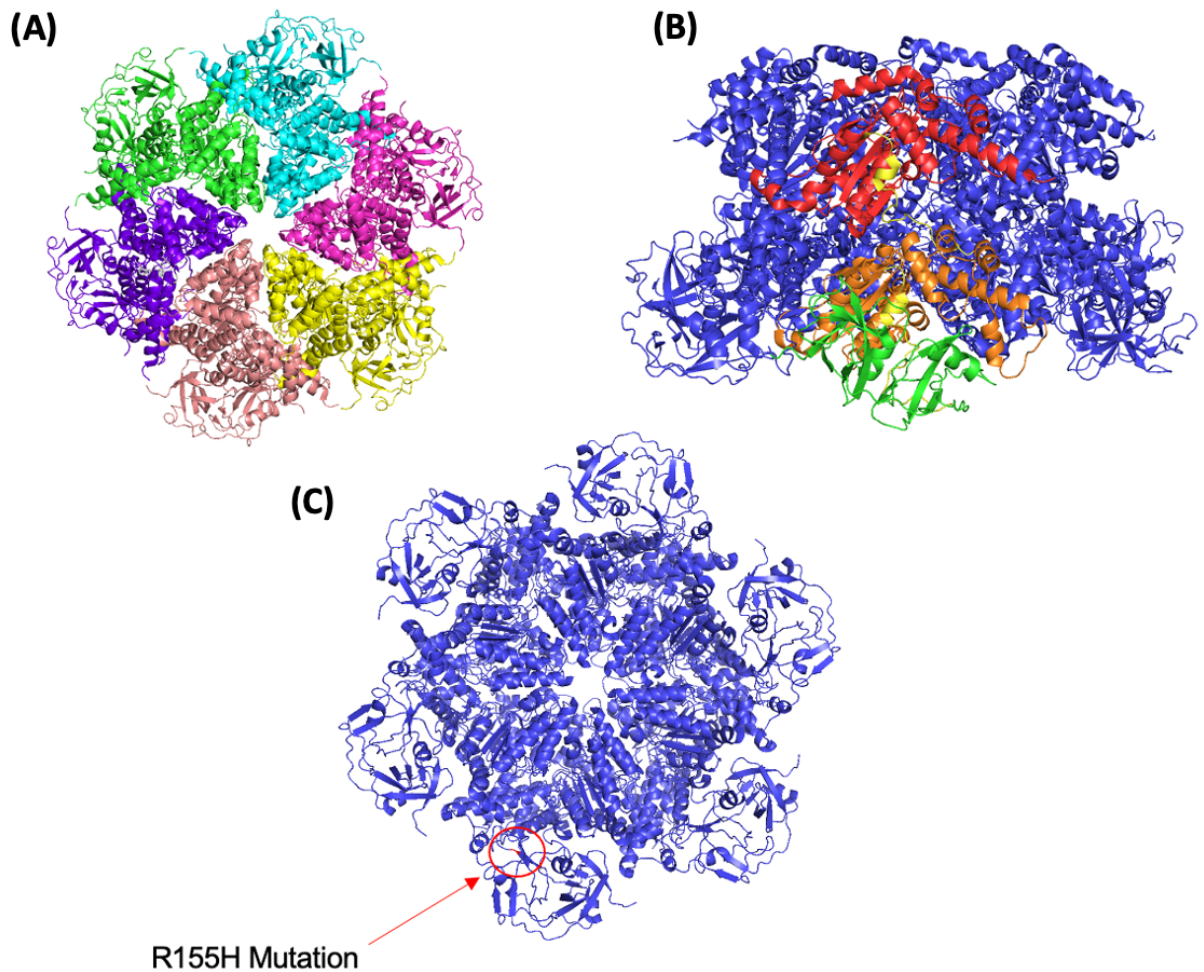


Figure 5- Valosin Containing Protein (VCP) structure (PDB: 5FTK (A,B) 7RL6 (C)).(A) Hexameric configuration demonstrated by various colors. (B) Components of each individual monomer distinguished through a green labeled N domain, orange labeled D1 domain, red labeled D2 domain, and yellow linkers. (C) Pathogenic R155H mutation implicated in relevant cell model of MSP-1, color coded in magenta and labeled.

VCP is a conserved AAA-ATPase which is associated with many cellular pathways and activities and is vital in maintaining cellular homeostasis. While the mechanism of VCP dysfunction has yet to be fully elucidated, literature suggests that these single missense mutations do not lead to a global loss of function, but rather, inhibit downstream functions of various cellular functions due to compromised association with certain cofactors.¹³ While there many functions of interest, due to the disease causing protein aggregates formed in MSP-1 patients, protein clearance

systems are of interest. The ubiquitin proteasome system (UPS) is responsible for the degradation smaller proteins and aggregate while autophagy is responsible for larger formations including dysfunctional organelles that the UPS is unable to process.¹⁴ VCP knockdown and mutant models have demonstrated defects in the clearance of ubiquitinated proteins, illuminating the possibility of a dysfunctional ubiquitin proteasome system (UPS) and/or improper autophagy.¹⁵

VCP Function in Protein Clearance

Out of the many substrates that bind to the peripheral N-domain of VCP, Ubiquitin-X (UBX) domain containing proteins are the largest family of cofactors as VCP plays a crucial role in UPS and quality control of ubiquitinated proteins in the proteasome.¹³ Because of this governance, VCP protects cells from cytotoxic effects of damaged or misfolded proteins and is implicated in cellular stress response.¹⁶ Despite the vitality of VCP in the UPS and subsequent regulation of many cellular processes, there has been discourse over if VCP mutations cause dysfunction of the UPS with literature reporting that disease causing protein aggregates form as a result of dysfunctional autophagy, not UPS defects. Although one of the hallmark pathologies of MSP-1 is ubiquitin positive accumulations, it is suggested that rather than dysfunctional UPS clearance causing these aggregates, VCP may play a selective role in the clearance of ubiquitinated substrates.¹⁷

Autophagy is a conserved, cell degradation process which is essential to removing dysfunctional components and maintain cellular homeostasis. It occurs via a lysosomal pathway with VCP being mainly involved in macroautophagy. This recycling and degradation process comprises of 4 steps: initiation, elongation, maturation, and degradation with VCP being implicated in initiation and maturation. Additionally, VCP has been identified in the transcriptional

regulation of genes involved in both autophagy and inflammation.¹⁸ In mutated VCP cell models, autophagosomes are unable to mature into lysosomes and undergo enzymatic degradation leading to accumulation of the disease-causing ubiquitin positive autophagosome aggregates.¹⁷

Relationship between Autophagy and the Ubiquitin Proteasome System

While autophagy and the UPS are not dependent on another, the two systems exist in a complementary relationship. When one system is inhibited or unable to clear misfolded, disordered, or aggregated proteins the other system will compensate through upregulation.¹⁹ Autophagy upregulation does not require total inhibition as even slight impairment of the UPS leads to a up regulated autophagic response.²⁰ It has also been demonstrated in a *Drosophila* model of proteasome impairment, that induction of autophagy can compensate for such proteasome impairment and suppress degenerative phenotypes.²¹ However, in models such as MSP-1 where autophagy is compromised, the UPS system becomes overwhelmed, and the cell no longer has adequate protein clearing machinery. Given the synergism of cellular protein clearance pathways and the degenerate nature of MSP-1, it is hypothesized that phenotypic improvement may occur with agents that modulate autophagy, cellular stress, and inflammation.

Therapeutic Approach

Under the working mechanistic hypothesis stated above, two therapeutic approaches were employed: 1) restoration or improvement of autophagic function, and 2) attempts to reduce or prevent UPS impairment by reducing cellular stress. The first therapeutic approach targets the autophagy pathway with aims to improve or restore function. **Rufinamide**, which is an FDA approved orally bioavailable agent (epilepsy) was chosen as an autophagy inducing agent due to previous work done in the Gavegnano lab for the repurposed application in the setting of HIV-1. The published mechanism of rufinamide is largely unknown towards its anti-epileptic effects, and loosely reported to modulate sodium channel induction (Rufinamide package insert). While not chosen as agents to study in this method development due to unfavorable safety profiles *in vivo*, Rapamycin has established autophagic functions and will serve as an insightful positive control.

The second therapeutic approach is twofold: restoration of cellular homeostasis to prevent UPS impairment causing subsequent use of autophagy for protein clearance and reducing directing signals to the autophagic pathway. Oxidative stress occurs when there is an excess of reactive oxidative species (ROS) due improper equilibrium of production and usage or detoxification of these species.²² In the current disease state, oxidative stress was of particular interest due to increase in protein aggregation due to UPS impairment, for which these aggregates can then cause an increase in ROS production- promoting a vicious cycle.¹⁸ Notable producers of ROS in many cells are the NAPH oxidases (NOX1-5 and DUOX1-2) which have become prime therapeutic candidates to target elevated ROS levels in disease associated with oxidative stress. NOX inhibitors have recently been recognized as a new therapeutic class, and show excellent promise due to their specificity to target ROS production without interfering with other cellular processes.²³ 3 NOX Inhibitors in various stages of development were chosen; **Setanaxib**, **APX-115**, and

GKT 136901. Setanaxib (GKT137831) was the first NOX inhibitor enter clinical trials and is a selective NOX1/4 dual inhibitor ($K_i=140\pm 40/110\pm 30$ nM). It is currently being investigated for various indications such as primary biliary cholangitis (phase 2), 2 diabetes and albuminuria (phase 2), and more as it has shown to significantly decrease levels of fibrosis and inflammation in relevant models.²⁴ In addition to Setanaxib, there are several other NOX inhibitors currently under development and in clinical trials. In addition to being a NOX1/4 dual inhibitor ($K_i = 160/165$ nm), GKT136901 is a select and direct scavenger of peroxynitrite, and was chosen based off this additional property of interest and potential benefit²⁵. Lastly, APX-115 was the first-in-class pan-NOX inhibitor with the ability to inhibit NOX1,2,4 ($K_i = 1.08 \mu\text{M}$, $0.57 \mu\text{M}$, and $0.63 \mu\text{M}$) and has shown similar or improved broad inhibition of NOX isoforms compared to Setanaxib in diabetic mice.²⁶

Inflammation was next considered to reduce cellular stress, and transcription factor NF- κ B became of special interest as VCP has been shown to regulate its activation, which can lead to upregulation of autophagy.^{18, 27} The exact mechanics of this interaction is unknown, and could serve as a novel target and prove useful in other diseases in which NF- κ B is implicated. Additionally, NF- κ B and ROS production are closely linked as ROS can activate NF- κ B. The interplay between NF- κ B towards ROS production is key in this disease setting, and thus blockade of ROS by NOX inhibitors provides a mechanism to block the downstream effects without directly targeting the highly promiscuous NF- κ B pathway. To complement the NOX inhibitors which seek to inhibit ROS production, Baricitinib, a JAK-STAT inhibitor (Jak 1/2 selective) was chosen to target inflammation and the NF- κ B implicated pathway.²⁸ The JAK/STAT pathway was first described in the 1990s and has a well-established role in immune signaling with evidence to support alternative mechanisms during times of cellular stress.²⁹

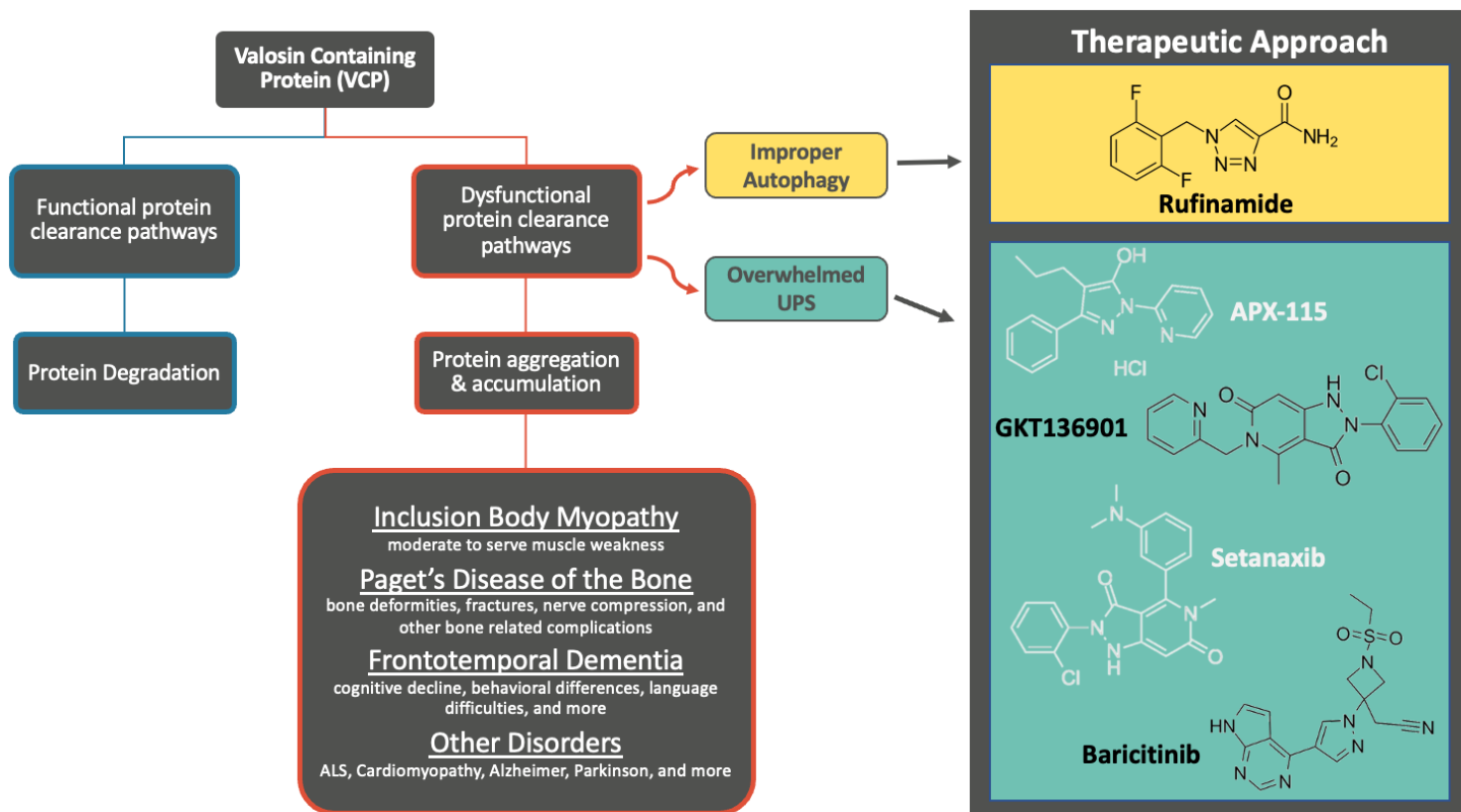


Figure 5- VCP regulates protein degradation pathways which are targeted to reduce or reverse phenotypic outcomes.

Methods

Initial Cell Culture

A fibroblast cell line was obtained from an individual clinically affected with Inclusion Body Myopathy with Early Onset Paget Disease, possessing the pathogenic R155H mutation which was ordered from Coriell Institute (GM23290). Once arrived, the attached protocol was

followed. Cells arrived in media, in a T25 flask with instructions to incubate for 36 hours without opening. After 36 hours had passed, cells were passaged by first removing media from the flask via stereological pipette and storing for future use. Cells were examined under a microscope and determined to have 60-70% confluency. Given the adherent nature of fibroblasts, approximately 2mL of Trypsin/EDTA solution was added to the flask in a thin layer to entirely cover the bottom of the flask to promote detachment of cells from flask. This was placed in incubator (37 degrees, 5% CO₂) for about 8 minutes, checking every 2 minutes to check detachment of cells. After proper balling and detachment, the flask was forcibly, yet carefully hit to remove other cells from the bottom of the flask. ~8mL of previously removed, Fetal Bovine Serum (FBS) containing media was added to the flask to inactivate the trypsin. Cells were then counted using 10µL of 1:1 cell suspension, trypan blue dye using a Countess cell counter which recorded 0.183×10^6 cells at a viability of 54%. Cell suspension was carefully transferred into T25 flask and placed in incubator for 5 days to increase viability and allow for cell proliferation.

Cell Culture

Future cell culture methods followed similar protocol, but utilized prepared media of 15% FBS, 5mL of non-essential amino acids (NEAA), and 2% Penicillin-Streptomycin. After initial media was removed, a Hanks Balanced Salt Solution (HBSS) was used to rinse the cells. Approximately 3mL or enough to cover surface of Trypsin/EDTA as then placed on top of the rinsed cells in a thin layer to detach cells from flask surface, after proper detachment ~15mL (or approximal 5x the amount of trypsin used) of growth/stop media was added. Once stop media was added, cell suspension was transferred to 50mL conical tubes and centrifuged at 1500rpm for 7 minutes. Carefully avoiding pelleted cells, media supernatant was removed, and the pellet was

resuspended in fresh culture media at a plating density of $8.5 \times 10^5 - 1.3 \times 10^6$ per flask (provided by the Coriell institute protocol) in at least 13mL of media to cover the bottom of the flask. Media was transferred to T75 flask, as volume of cells increased from arrival. Due to the fast-growing nature of these cells, passaging occurred approximately every 3 days to prevent over confluency and cell death. Cells were either passaged to new T75 flask or frozen at a density of approximately 2 million cells/mL freezing solution.

Freezing

Similar protocol was followed as cell passaging, however, instead of adding fresh media after centrifugation freezing media was added. Freezing media consists of 90% FBS/10% DMSO. With a desired density of 2 million cells/mL freezing media, proper amounts of media was prepared. Cells suspended in freezing media were transferred to cryogenic tubes for freezing, these tubes were promptly placed in the -80°C freezer in a freezing container. Such freezing container was used to achieve a $-1^{\circ}\text{C}/\text{minute}$ cooling rate for optimal cell preservation and to prevent sudden cell death. After 24-48 hours in freezing container at -80°C , tubes were transferred to -150°C freezer.

Plating Density

Prior to conducting validation assays, fibroblast plating density was optimized in 96 well plates by plating various densities of cells, observed over several time periods over 5 days. Cells were plated at densities of 5, 10, 15, 20, 25, 50,000 cells per well and were examined at 24,48,72, 144-hour time stamps. Due to the fast growing and voluminous nature of fibroblasts, 5,000 cells

per well was determined to be optimal to prevent over confluency and cell death, demonstrated in Figure 6.

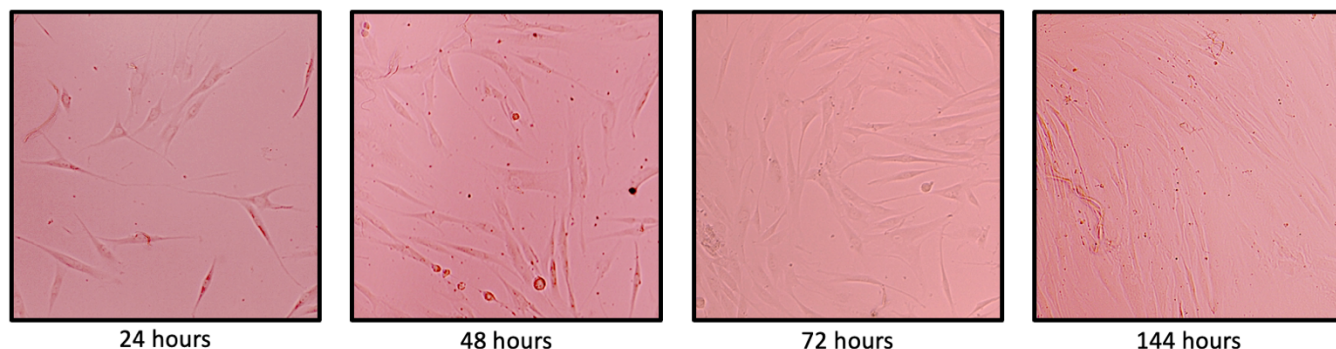


Figure 6- 5,000 Cells per well initially established as optimal

Various densities were plated and observed over 24,48,72, and 144 hours to determine optimal density for toxicity and efficacy assays. 5,000 cells per well was considered optimal as all other values resulted in over confluency and subsequent cell death.

After facing difficulties with assay wobble and inconsistency due to cell behavior, which was possibly a result using of previously frozen cells and/or plating discrepancies due to extended trypsin contact, the density was reoptimized. Using freshly thawed cells, plated directly into a 96 well (as opposed to acclimating to T75 flask and then transferring to 96 well plate) a decreased density of 2,500 cells/well illustrated proper confluency and behavior, demonstrated in figure X. The morphology of the fibroblasts appeared altered after cryogenic storage, with shorten height and width (thus a net decrease in surface area) and increased presence of spherical cells. While this was of initial concern, this concern was dismissed by high cell viability (>70%), maintained adhesive properties, and similarity to reference image of early passage fibroblasts isolated from human dermal cells.³⁰ Additionally, as time progressed cells restored similar morphological properties, demonstrated in figure X. adapted from Stem Cells and Good Manufacturing Practices, 2020.

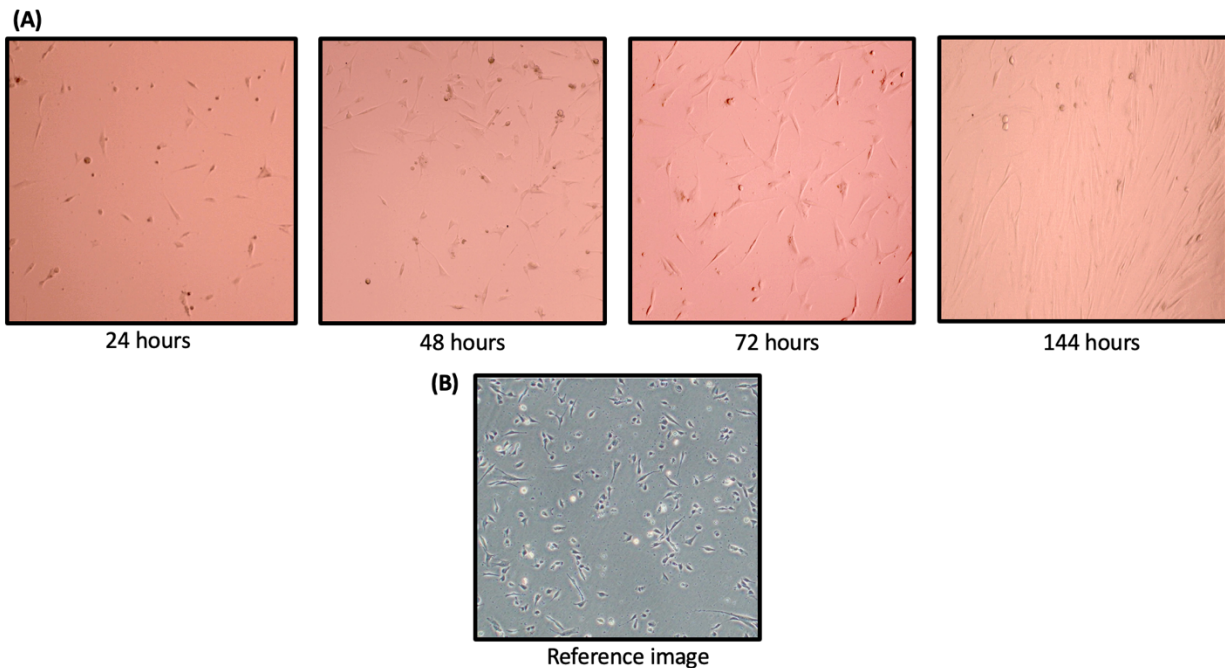


Figure 7- Determination 2,500 cells/ well as optimal plating density of freshly thawed cells. (A) 2,500 cells/ well at various time points. Previously frozen, now freshly thawed cells were plated directly into 96 well plates. (B) Reference image of early passage fibroblasts derived from human skin (adapted from Stem Cells and Good Manufacturing Practices, 2020).

MTS Assay

To establish a therapeutic window of safety, cytotoxicity of various inhibitors was tested via a MTS cell proliferation colorimetric assay. Cells were plated at a density of 2,500 cells/well in a 96 well plate and treated with inhibitors of choice at concentrations of 10^1 , 10^0 , 10^{-1} , 10^{-2} , 10^{-3} , 10^{-4} , 10^{-5} , 10^{-6} , 10^{-7} μM in 200 μL of growth media. The positive control for cell death were cells treated with DMSO beginning with a 50% DMSO, 50% growth media solution with a subsequent 2-fold dilution down the row ending with concentration 0.39% DMSO, 99.61% growth media solution. Positive control cells were remained in growth media. Cells were incubated for 5-7 days and then treated with 10 μL per well of MTS reagent dye for approximately 1 hour or

until visual changes occurred. Visual changes of interest were a yellow color to the DMSO lanes and purple color for all other lanes, denoting viability (purple MTS tetrazolium reaction), or cell death (uncleaved reagent; dead cells). The plate was then analyzed using the Synergy microplate reader to measure optical density with absorbance at 490 nm (BioTek Instruments).

Reactive Oxidative Species (ROS) Detection & Optimization

To understand the efficacy of NOX Inhibitors and other therapeutic agents, ROS levels were measured using Total Reactive Oxygen Species (ROS) Assay Kit ordered from ThermoFisher. Cells were plated in a 96 well at an optimized density of 2,500 cells per well and incubated for a day to allow cells to acclimate. Cells were then treated with 1 μ M and 0.1 μ M concentration of therapeutic of interest and incubated for time points of interest (1 and 24 hours; known time points associated with ROS production/inhibition and detection). Next, cells were stained with prepared stock solution of ROS Assay Stain, purchased from Invitrogen. Solution was prepared by adding 40 μ L of DMSO to purchased assay stain concentrate which yielded a 500X stock solution. This stock was then diluted to an optimal 1X concentration in ROS assay buffer. After proper incubation, drug solution was removed from cells 100 μ L/well of ROS assay stain was added to treated cell and incubated for 1 hour. Fluorescence was then measured using a Synergy microplate reader set to excitation at 48nm and emission 520nm.

Autophagy Assay

To understand the role of stress prevention on autophagy and potential impact of Rufinamide in restoring autophagic function, an autophagy assay kit from Abcam was utilized. Pre-assay preparation included reconstitution and dilution of controls (Rapamycin and Chloroquine), assay buffer, and green/blue detection reagents according to assay protocol.

Experimental cells were plated at an optimized 2,500 cell/ well density and treated with 1 μm and 0.1 μm concentrations at time points of interest (18 and 24 hour). Control cells were treated with 0.5 μM Rapamycin and 10 μM Chloroquine. 10X assay buffer was diluted to 1x and use to rinse cells after treatment was removed (100 μL per well to rinse). A dual stain solution was prepared, with of 1 μL of Green Detection Reagent and 1 μL Nuclear Stain being added to every 1mL of phenol red-free cell culture media. 100 μL of this stain solution was added to each well and incubated at 37 C°. After, cells were washed twice with 200 μL of 1x assay buffer, 100 μL of buffer was added for analysis. Analysis was conducted using the Synergy fluorescence plate reader with green fluorescence measured at 480 nm excitation, 530 nm emission and nuclear stain was measured at 340nm excitation and 480 emissions.

Results

Toxicity Screening

All five compounds were screened for toxicity using, an MTS to measure cell viability. Results were reported in % inhibition of cell growth relative to control cells (media alone; control for no cell death). In scenarios in which there was a negative % inhibition (the growth of the drug treated cells exceeded the growth of the control cells), the value was normalized to 0. A summary of all tested compounds and individual compound results are included below as Figures 8 and 9, receptively.

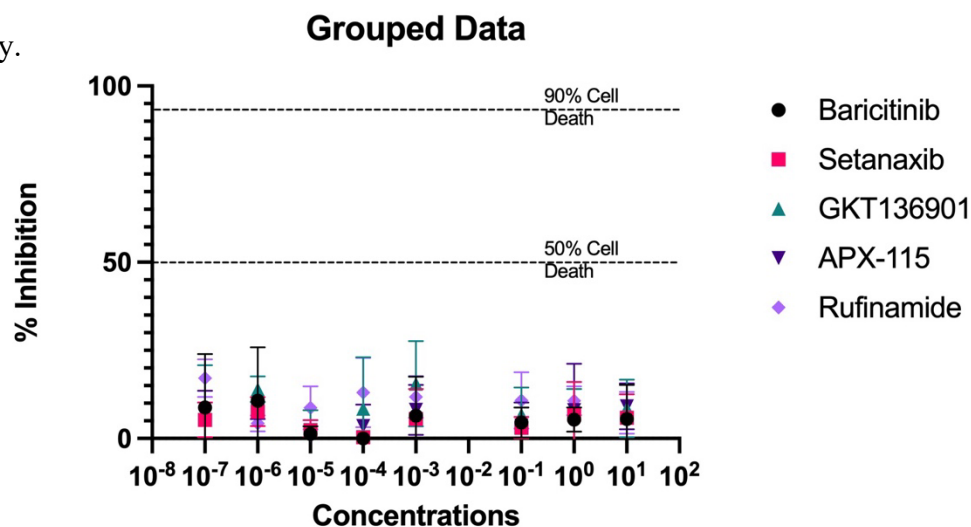


Figure 8-Summary of compound cytotoxicity assessed by MTS assay. Expressed as percent inhibition of cell growth relative to untreated controls cells. Cells treated with compounds at concentration range 10^{-7} - 10^1 μM for 5-7 days. Error bars indicate standard deviation.

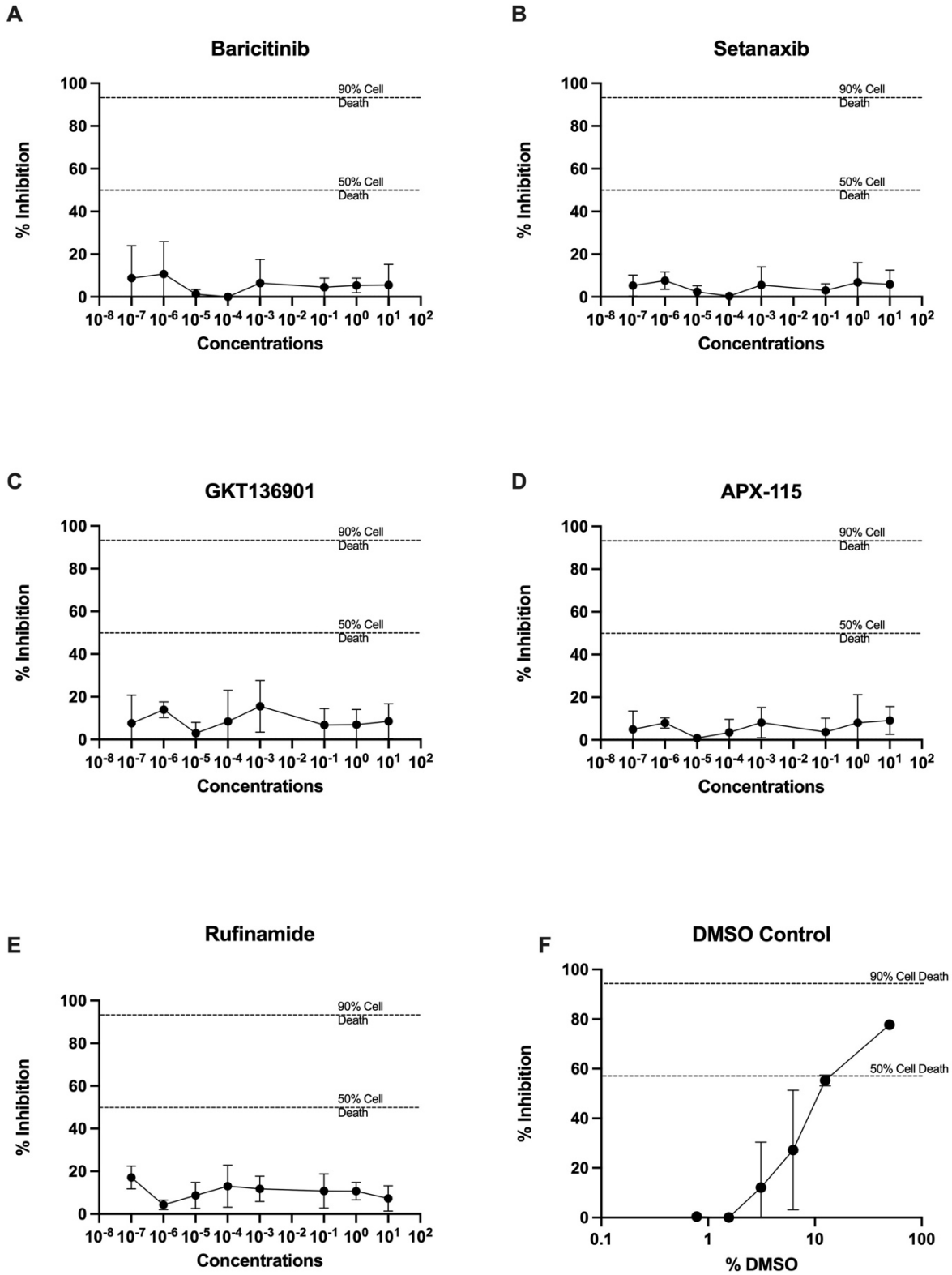


Figure 9-Compounds of interest do not inhibit cell growth assessed by MTS assay, expressed as percent inhibition of cell growth relative to untreated controls cells. Cells treated with compounds at concentration range 10^{-7} - 10^1 μM for 5-7 days.. (A)Baricitinib (B) Setanaxib (C) GKT136901 (D) APX-115 (E) Rufinamide (F) DMSO Control. Experiments done in duplicates over 3 biological replicates. Error bars indicate standard deviation.

Autophagy Studies

The decision to investigate Rufinamide as an autophagy inducer was driven by previous work done in the Gavegnano lab has demonstrated the ability of Rufinamide to induce autophagy markers and autophagosome formation in D3HIV-GFP vector transduced monocyte- derived macrophages, demonstrated in Figure 10. ³¹

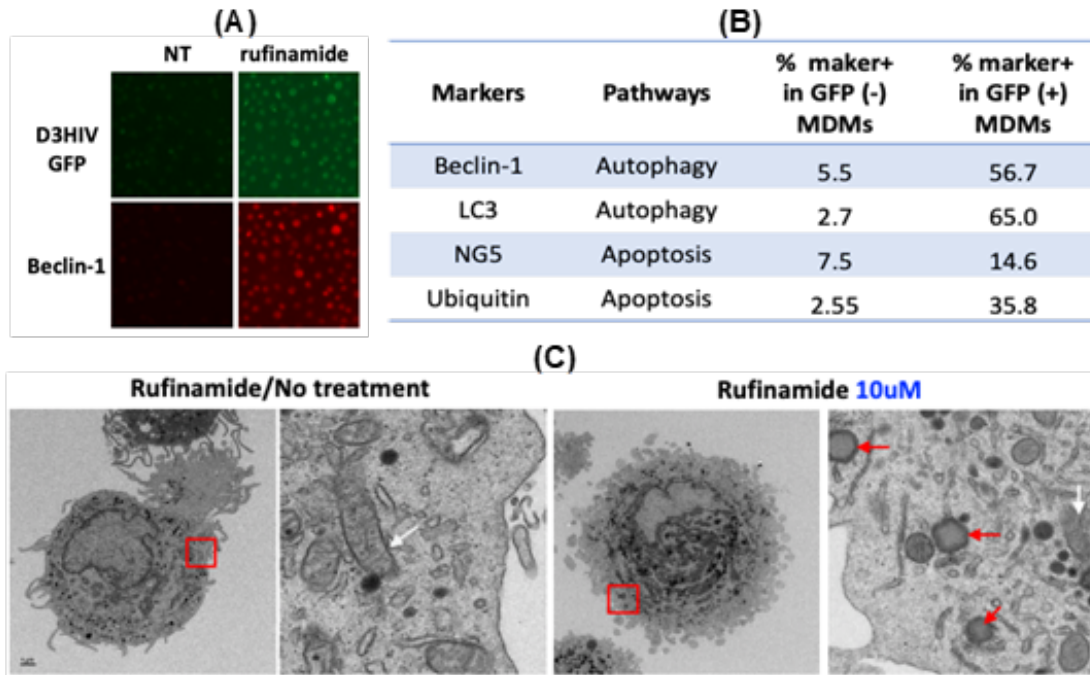


Figure 10- Effect on rufinamide on autophagy and apoptosis marker activation and autophagosome induction in HIV-1 vector transduced MDMs. Beclin-1 (A) and LC3 autophagy markers and NG5 and Ubiquitin apoptosis markers (red) were stained and FACS-analyzed (B) in D3HIV-GFP vector transduced (GFP+) and untransduced/internal negative control (GFP-) MDMs upon rufinamide treatment (10 μ M). (C) EM analysis was conducted for autophagosome detection in MDMs transduced with D3HIV- GFP (M OI 2) with and without rufinamide treatment at 4 days post transduction. Red box areas in 1 μ M pictures were zoomed for detecting organelles. Red arrows: autophagosomes with double (thick) membrane structures. White arrows: mitochondria. Adapted from M. Reece.

Rufinamide along with all other compounds being screened, were also screened for their abilities to induce, or inhibit autophagy. Initial screening occurred at 0.1 and 1.0 μ M for 18 and 24 hours with 10 μ M Chloroquine and 0.5 μ M Rapamycin serving as controls as instructed by assay

manual. Autophagic vacuoles were stained with a green detection agent and cell nuclei were stained with blue nuclear dye. Data was normalized by using both stains to quantify green fluorescence relative to blue fluorescence to account for plating and other cellular inconsistencies.

Images were collected after Synergy plate reader analysis (Figure 10), however, after extended time in buffer solution cell morphology began to shift and appear in a more spherical shape. This was a result of the buffer, as demonstrated by Figure 10B, in which non-treated, non-stained cells exhibited a similar morphology after sitting in buffer for 1 hour. In order to gain a better visual understanding, additional cells were treated, stained, and imaged in color free growth media under individual DAPI and GFP filters, and then merged to obtain 3 distinct, informative images (Figure 11).

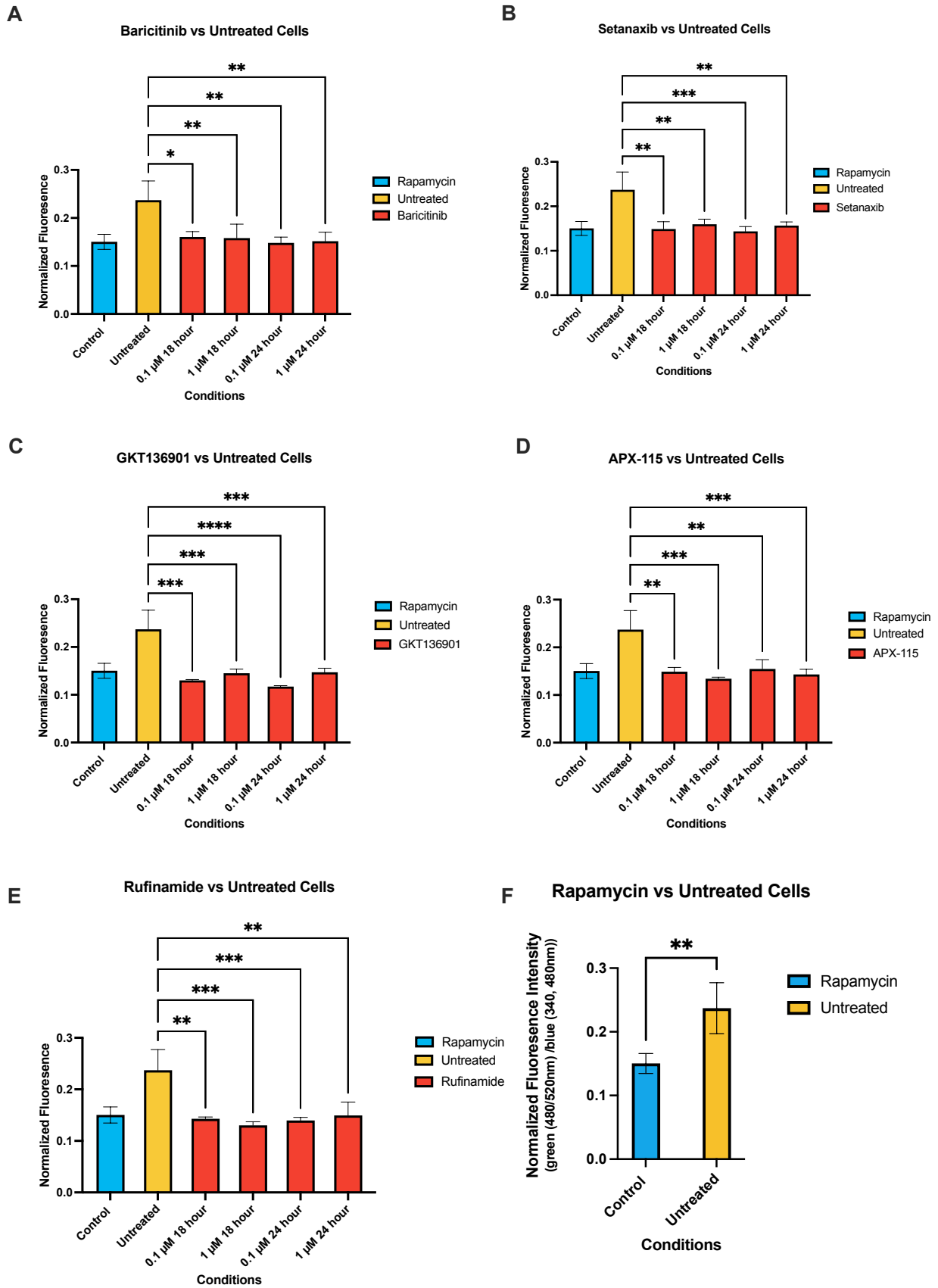


Figure 11- Compounds of interest reduce autophagic vacuole accumulation. Normalized Fluorescence reported as green fluorescence/blue fluorescence. (A) Baricitinib (B) Setanaxib (C) GKT136901 (D) APX-115 (E) Rufinamide (F) Rapamycin positive control. One-way ANOVA with multiple comparisons was used. Error bars indicate standard deviation, $p > 0.05 = \text{n.s.}$, $p \leq 0.05 = *$, $p < 0.01 = **$, $p \leq 0.001 = ***$, $p \leq 0.0001 = ****$.

Compound	Class	Condition	P Value
Baricitinib	Jak 1/2 inhibitor	0.1 μ M, 18hr	0.0117
Baricitinib	Jak 1/2 inhibitor	1 μ M, 18hr	0.0096
Baricitinib	Jak 1/2 inhibitor	0.1 μ M, 24 hr	0.0045
Baricitinib	Jak 1/2 inhibitor	1 μ M, 24hr	0.0059
Setanaxib	NOX 1/4 inhibitor	0.1 μ M, 18hr	0.0014
Setanaxib	NOX 1/4 inhibitor	1 μ M, 18hr	0.0037
Setanaxib	NOX 1/4 inhibitor	0.1 μ M, 24 hr	0.0009
Setanaxib	NOX 1/4 inhibitor	1 μ M, 24hr	0.0028
GKT139601	NOX 1/4 inhibitor	0.1 μ M, 18hr	0.0001
GKT139601	NOX 1/4 inhibitor	1 μ M, 18hr	0.0004
GKT139601	NOX 1/4 inhibitor	0.1 μ M, 24 hr	<0.0001
GKT139601	NOX 1/4 inhibitor	1 μ M, 24hr	0.0005
APX-115	Pan NOX inhibitor	0.1 μ M, 18hr	0.0014
APX-115	Pan NOX inhibitor	1 μ M, 18hr	0.0004
APX-115	Pan NOX inhibitor	0.1 μ M, 24 hr	0.0023
APX-115	Pan NOX inhibitor	1 μ M, 24hr	0.0009
Rufinamide	Potential Autophagy Inducer	0.1 μ M, 18hr	0.0012
Rufinamide	Potential Autophagy Inducer	1 μ M, 18hr	0.0005
Rufinamide	Potential Autophagy Inducer	0.1 μ M, 24 hr	0.0009
Rufinamide	Potential Autophagy Inducer	1 μ M, 24hr	0.0020

Table 1: P Values from Figure 11 statistical analysis (one way ANOVA).

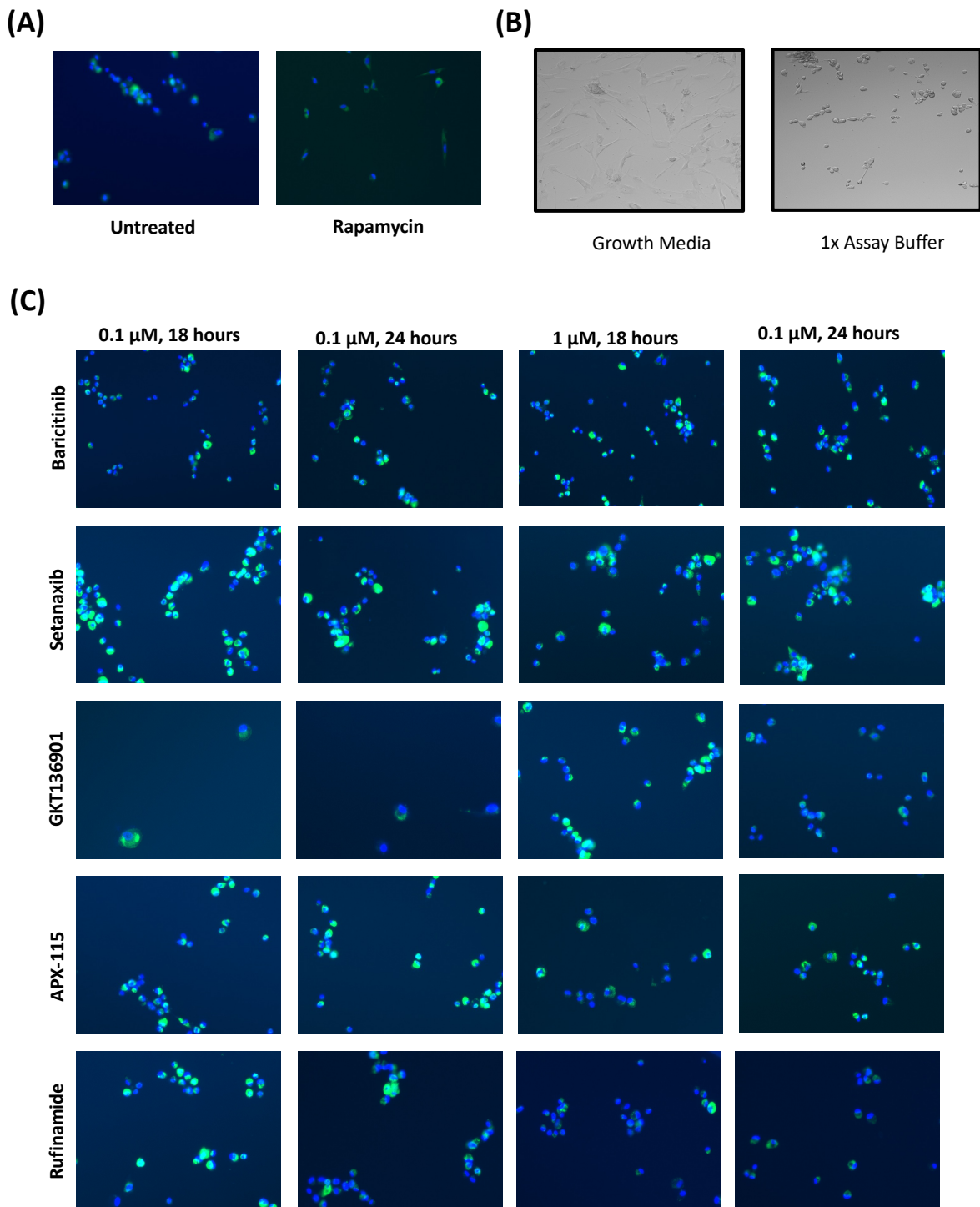


Figure 12- Autophagy assay staining visualization. Autophagic vesicles are stained green, while nuclear staining appears blue. Images taken with DAPI and GFP filter, merged together using EVOS software. (A) Untreated and Rapamycin positive control treated cells. (B) Untreated, unstained cells in growth media and assay buffer after 1 hour to demonstrate impact of buffer on morphology. (C) Various compounds at different conditions visualized.

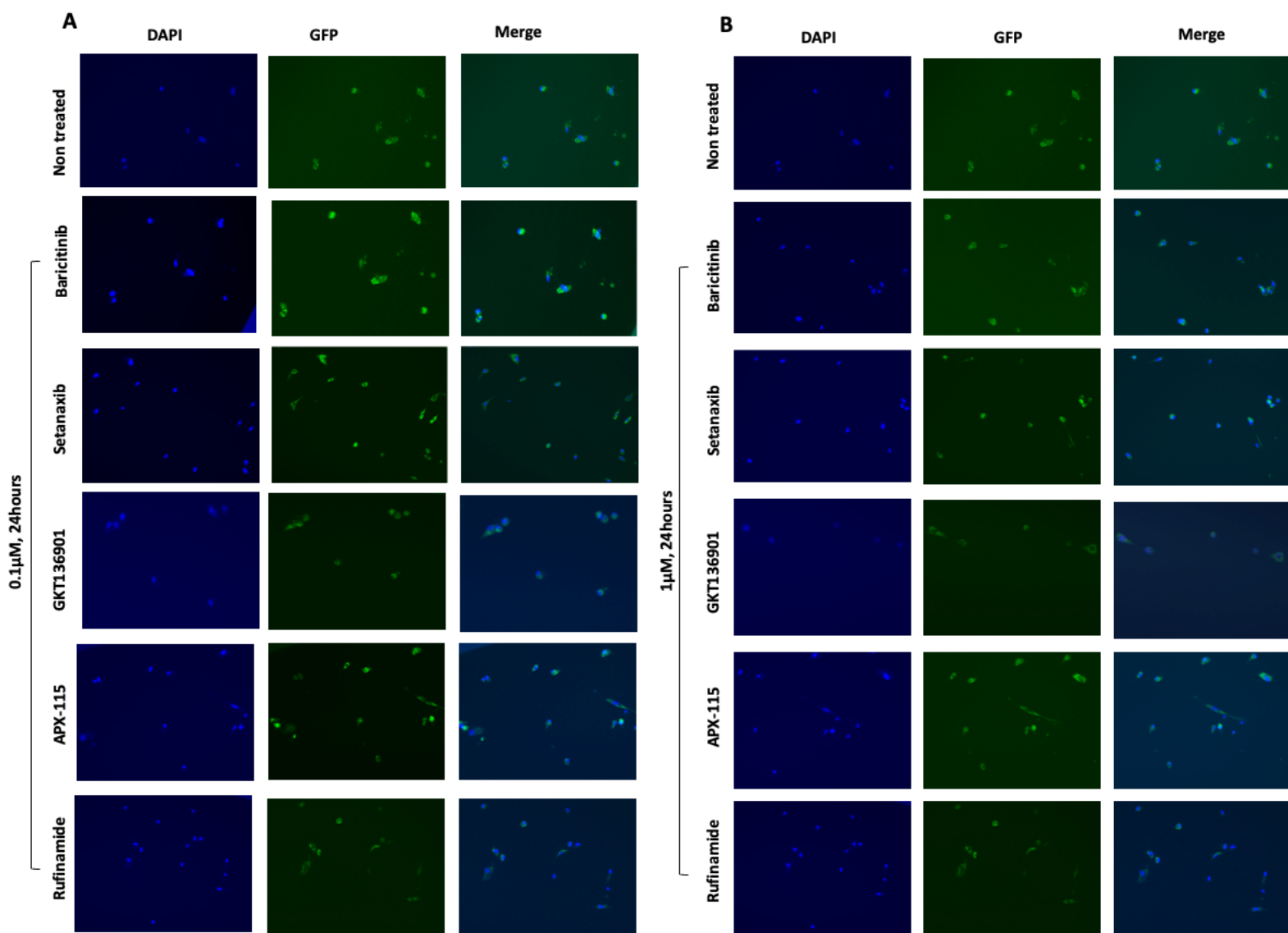


Figure 13- Additional staining conducted in growth media for improved visualization. DAPI and GFP filtered images were individually collected and then merged using EVOS software. (A) Cells treated with 0.1 μM of various compounds for 24 hours (B) Cells treated with 1.0 μM of various compounds.

ROS Detection

The detection of ROS in optimized conditions proved to be a difficult and is still an ongoing point of optimization. However, the preliminary data was promising and sparked interest in further optimizing and developing methods to detect ROS production in the dysregulated MSP-1 cells and inhibitory capabilities of various compounds.

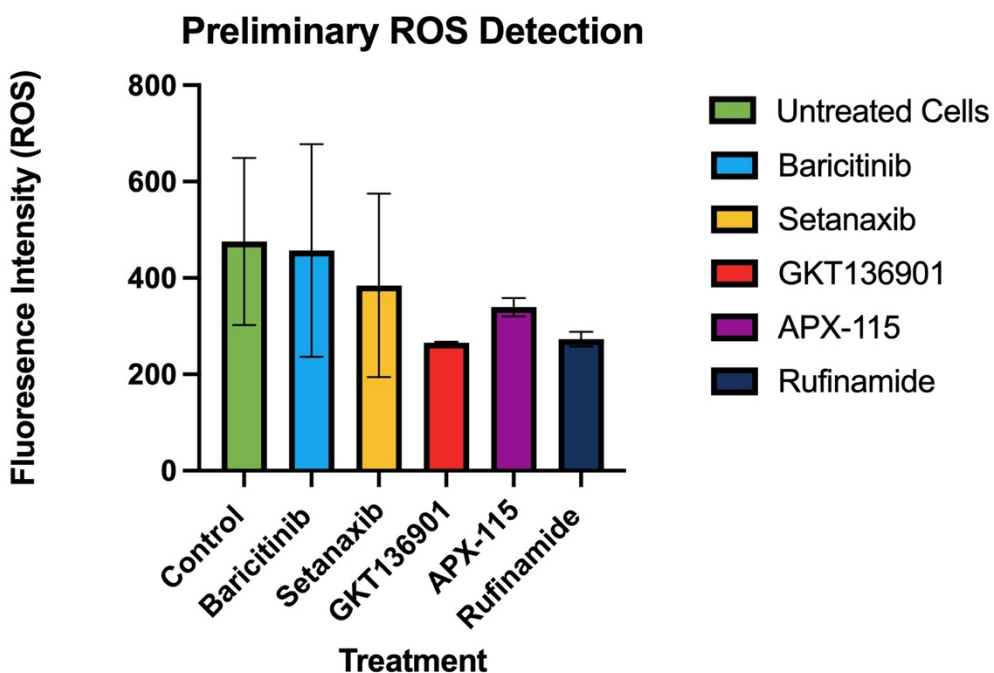


Figure 14-Preliminary data suggests potential inhibition of ROS production by various compounds in dysregulated MSP-1 cells. Error bars signify standard deviation.

To help reduce or account for wide variability in measurements and further study the properties of these compounds on ROS inhibition, we sought to optimize and validate the method. A first attempt in optimization was implementing a rinse step, inspired from the literature and other protocols of other staining procedures. Given the red color of the ROS assay buffer (provided with assay kit) and complementary green fluorescence of the stained cells, we believed a rinse may be beneficial to both remove any excess dye and prevent any dampening of measured fluorescence.

It was determined that a Dulbecco's Phosphate Buffer Solution (DPBS) rinse and use of DPBS to remove any residual stain or color from buffer solution was crucial. This was confirmed by comparing fluorescence intensity measurements of drug-free cells in assay solution (buffer + stain) and measurements after rinsing those exact same cells with DPBS, which were vastly different and statically significant ($p=0.0003$). Due to variance in initial and final readings but similar ratios of such increases, a ratio paired T test was used. The same was done with cells in just buffer. Additionally, the rinse step further illuminated and quantified the difference between stained and non-stained cells to give a more accurate floor and ceiling reading for the assay.

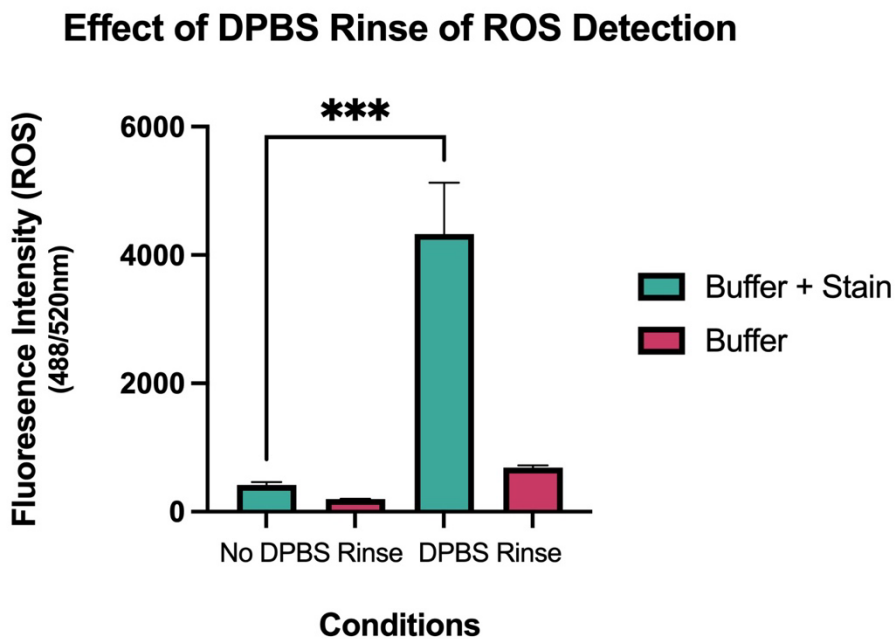


Figure 15- Optimization of ROS Assay- Effects of DPBS Rinse on ROS Detection. Cells treated with buffer + ROS detection stain were analyzed in buffer+ stain solution and after DPBS rinse 3x in DPBS. Repeated in buffer without stain. Ratio paired T test was used, $p=0.0003$, error bars indicate standard deviation. $p > 0.05 = \text{n.s.}$, $p \leq 0.05 = *$, $p < 0.01 = **$, $p \leq 0.001 = ***$, $p \leq 0.0001 = ****$.

The implementation of a wash step was beneficial to reduce variation between samples yet there is still difficulty in obtaining a consistent comparison value from the diseased cells. Even with this wash step, due to inconsistency of experimental samples, the current protocol utilizes a scaled control. Utilizing the relationship established between non stained and stained treatment-free cells from Figure 13, raw data from stained, non-treated and non-stained, no treated cells are compared and adjusted accordingly. As such, it is important to note that the control seen in Figure was not directly measured, but rather adjusted based off the same assay in a previous experimentation. These assays must be repeated for scientific rigor.

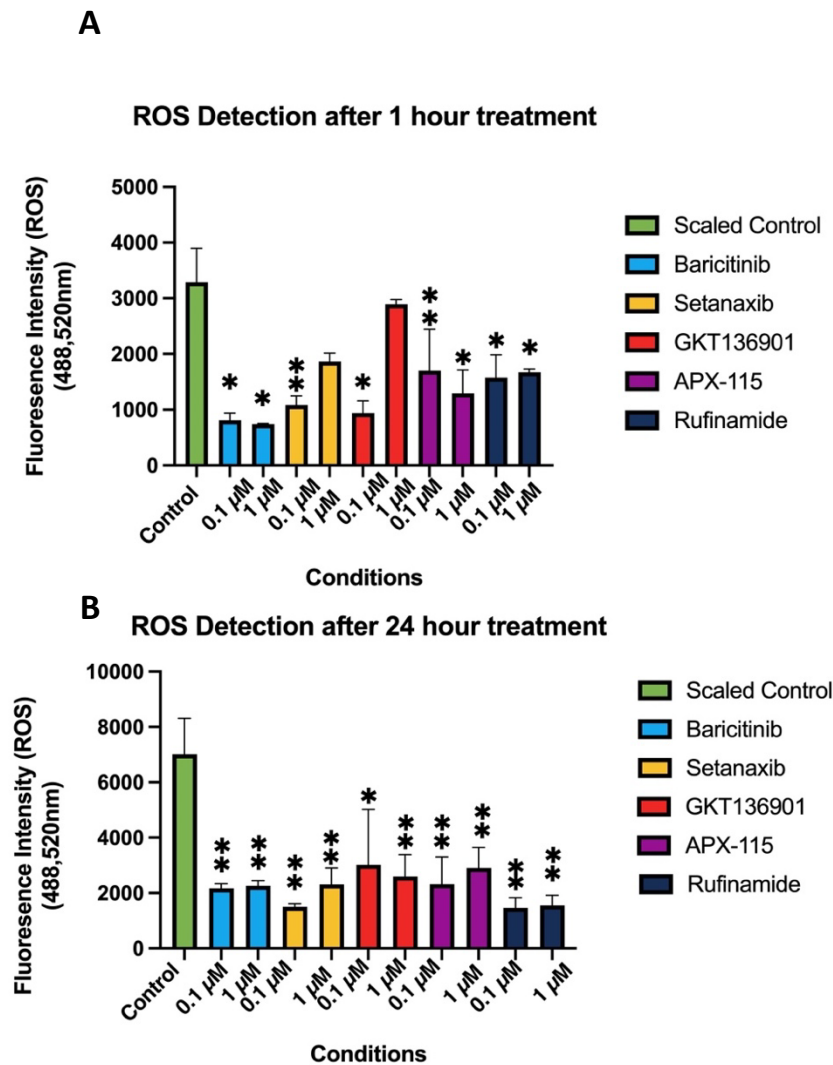


Figure 16- Compounds of interest inhibit production of ROS. Quantification of ROS by fluorescence intensity (488/520 nm). (A) Treatment of compounds for 1 hour at 0.1 and 1 μ M. (B) Treatment of compounds for 24 hours at 0.1 and 1 μ M. Unpaired T-Test was used for each condition, error bars represent standard deviation, $p > 0.05 = \text{n.s.}$, $p \leq 0.05 = *$, $p < 0.01 = **$, $p \leq 0.001 = ***$, $p \leq 0.0001 = ****$ 30

Compound	Class	Condition	P Value
Baricitinib	Jak 1/2 inhibitor	0.1 μ M, 1hr	0.0125
Baricitinib	Jak 1/2 inhibitor	1 μ M, 1hr	0.0112
Baricitinib	Jak 1/2 inhibitor	0.1 μ M, 24 hr	0.0031
Baricitinib	Jak 1/2 inhibitor	1 μ M, 24hr	0.0033
Setanaxib	NOX 1/4 inhibitor	0.1 μ M, 1hr	0.0038
Setanaxib	NOX 1/4 inhibitor	1 μ M, 1hr	0.0539
Setanaxib	NOX 1/4 inhibitor	0.1 μ M, 24hr	0.0019
Setanaxib	NOX 1/4 inhibitor	1 μ M, 24hr	0.0047
GKT139601	NOX 1/4 inhibitor	0.1 μ M, 1hr	0.0033
GKT139601	NOX 1/4 inhibitor	1 μ M, 1hr	0.4494
GKT139601	NOX 1/4 inhibitor	0.1 μ M, 24 hr	0.0444
GKT139601	NOX 1/4 inhibitor	1 μ M, 24hr	0.0074
APX-115	Pan NOX inhibitor	0.1 μ M, 1hr	0.0095
APX-115	Pan NOX inhibitor	1 μ M, 1hr	0.0458
APX-115	Pan NOX inhibitor	0.1 μ M, 24 hr	0.0076
APX-115	Pan NOX inhibitor	1 μ M, 24hr	0.0090
Rufinamide	Potential autophagy inhibitor	0.1 μ M, 1hr	0.0156
Rufinamide	Potential autophagy inhibitor	1 μ M, 1hr	0.0382
Rufinamide	Potential autophagy inhibitor	0.1 μ M, 24 hr	0.0021
Rufinamide	Potential autophagy inhibitor	1 μ M, 24hr	0.0022

Table 2: P Values from Figure 16 statistical analysis (unpaired t-test).

It was hypothesized that inconsistencies were a result in variance in cell plating so in an attempt to gain more consistent results, an internal standard in the form of a nuclear stain was implemented. The approach was inspired from the autophagy assay, and since there was no written protocol, a similar 1:1 ratio of blue: green dye was used when staining the cells. This approach provides a proof-of-principle that nuclear DAPI stain in the presence of the GFP dye for autophagy can be performed, and will now be evaluated in the Synergy Plate Reader to normalize cell counts across wells, thereby reducing variability and normalizing data to cell count. This plan is discussed as a future direction.

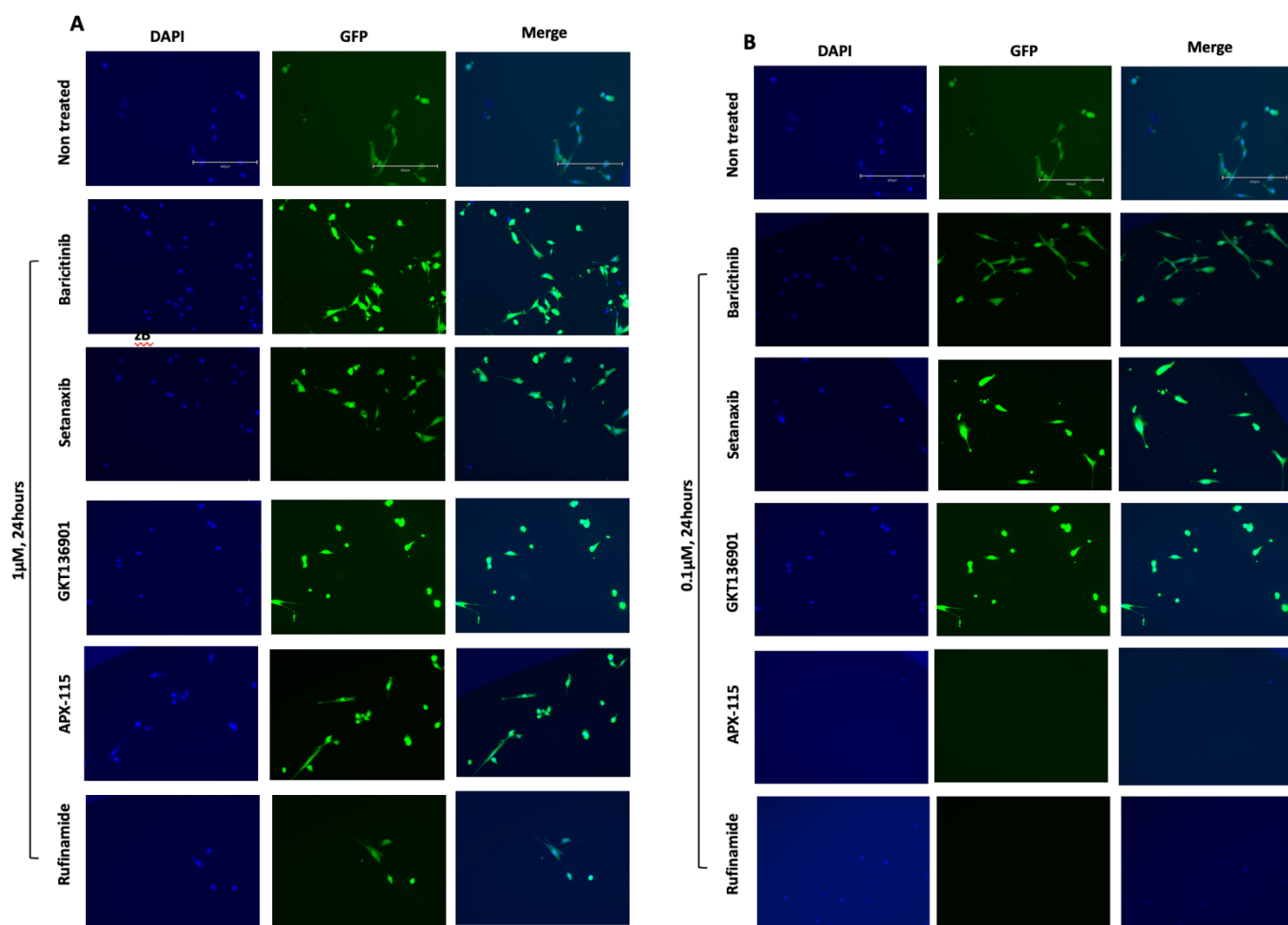


Figure 17- Blue nuclear staining as an internal control for ROS assay. Individual images taken with DAPI and GFP filters and then merged using EVOS software. (A) Cells treated at 1 μM for 24 hours. (B) Cells treated at 0.1 μM for 24 hours.

Discussion & Future Direction

Toxicity Studies

As demonstrated in Figures 8 and 9, all tested compounds at physiologically relevant concentrations in MSP-1 cells do not induce significant cell death, but also conferred efficacy in our preliminary screening systems, underscoring the potential for a wide therapeutic window of safety upon additional rigorous evaluation. Although the repurposed nature of these agents embodies a wide array of safety data and corresponding therapeutically relevant concentrations, these data mark the first time to our knowledge that these agents have been evaluated for toxicity (and efficacy) in a rare disease model. These data highlight a critical factor in drug discovery, wherein careful evaluation of toxicity across novel disease systems remains a first step in establishing eventual safety in humans across a novel indication.

Autophagy Studies

The autophagy assay kit used selectively labeled autophagic vesicles through green fluorescence and employed nuclear staining to normalize data. The data presented in Figure 11 and Table 1 demonstrate a significant decrease ($p < 0.05$, unpaired t-test) in autophagic vesicles present upon treatment with chosen compounds, mirroring the effects of rapamycin. With the current understanding that autophagy dysregulation stemming from the inability for autophagosomes to mature into autolysosomes, we believe the significant increase in fluorescence of the dysregulated MSP-1 cells compared to the drug-treated cells is due to accumulation of immature autophagosomes unable to complete total autophagy while drug treated cells are more able to complete such process and lack these accumulations. Studies have shown that treatment of rapamycin VCP^{R155H/+} mice lead to an improvement in the muscle pathology phenotype due, thus it is plausible the here-studied compounds could have similar effects.³²

Autophagy is a complex process, and the exact mechanism of how chosen agents enacted this change is unknown, but the use of Rapamycin provides insights to guide initial thoughts and future directions of mechanism elucidation. Rapamycin induces autophagy via mTOR inhibition, a protein that regulates autophagy initiation activation.³³With these this pathway in mind, future directions include further studies to understand where in the autophagic pathway chosen compounds aid in the clearance of autophagic vesicles and other mechanistic studies.

ROS Detection

While the chosen agents show promising results, this arm of the project focused on method optimization and proper quantification of ROS and/or inhibitory properties of the chosen compounds. DPBS rinse was proven to be vital to remove any excess dye after staining, increasing the difference in measured fluorescence intensity between stained and non-stained cells. However, even with the implementation of such rinse step- there was still significant assay wobble and difficulties in collecting consistent measurements. This wobble and inconsistency were hypothesized to be a result in plating. To target this hypothesis, the use of a nuclear staining was implemented in an attempt to utilize an internal standard for cell counting and normalization of cell counts across wells to fluorescence measured for the autophagy marker. Quantification of cells via staining to use a ratio metric of ROS was considered in the late stages of method development so there is significant room for improvement and further experimentation. Staining optimization such as ratio of blue nuclear stain to green-fluorescent ROS tagging, staining duration, use of specific stains, and vehicle for staining (buffer, media, etc) are just a handful of considerations and experiments which will be conducted in the future. Once fully optimized and functional, we

believe the assay could be extremely beneficial in detecting ROS in other rare and orphan diseases, since ROS plays a pivotal role in many diseased states.

Rare and Orphan Disease Drug Discovery

The development of drug discovery platform focusing on rare and orphan diseases required substantive intentionality and creativity to overcome challenges and barriers. Based off challenges and advancements, a workflow was created to assist in future projects and the continuation of this platform as summarized in Figure 18.

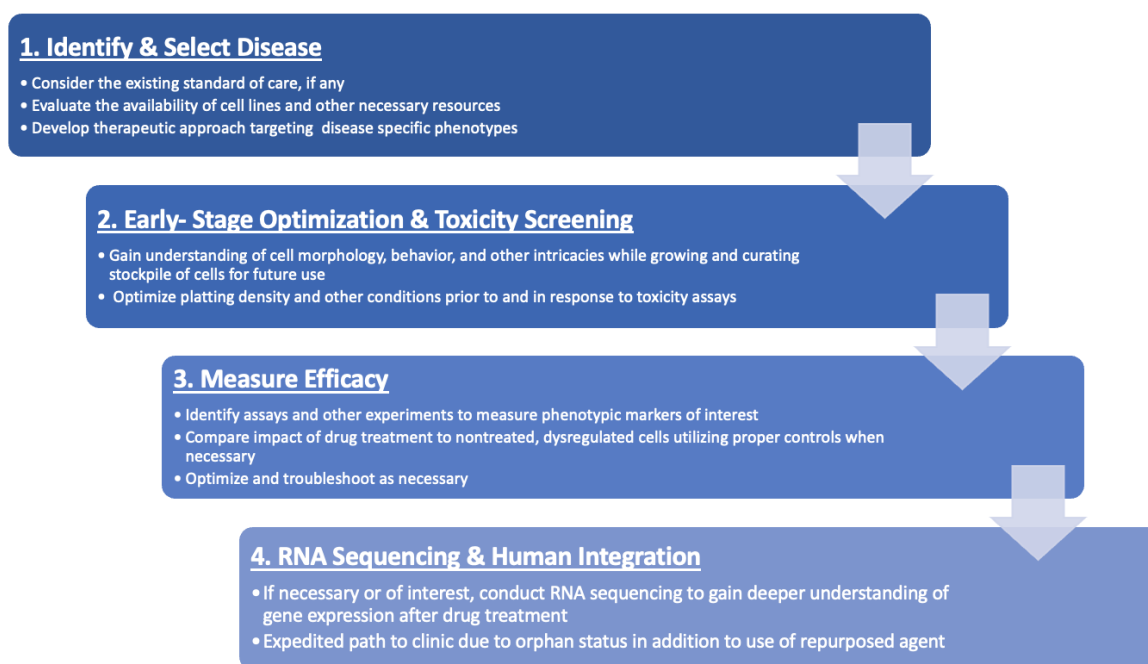


Figure 18-Workflow for rare and orphan drug discovery

Beginning with disease identification, a sizeable library of prospective diseases was initially curated based off phenotypes, yet cell line availability was limited to a handful of diseases. With this in mind, cell line and other resource availability and accessibility must be considered when working with rare diseases. After confirming cell line availability, extensive literature search began to gain a better understanding of molecular, phenotypic, and genetic basis of the chosen

disease to generate an informed therapeutic approach. While the therapeutic approach is primarily diseases driven, it is also important to consider existing standards of care (if any) in addition to bioavailability, toxicity, and relevant side effects of compounds of interest. To compliment the already existing safety data for repurposed agents, toxicity screening occurred to validate the safety of the selective compounds in a specific cell line. After safety was established, planning and implementation of efficacy screening began. In the case of MSP-1 preliminary efficacy studies focused on autophagy and ROS detection. Depending on the outcomes and results of these experiments, additional experiments may be conducted to test new hypothesis or further elucidate mechanism of interest. If such studies provide promising results, it may be beneficial to submit drug treated samples for RNA sequencing to gain a better understanding of gene expression. RNA sequencing for the disease at hand (MSP-1) has been discussed and is of interest after additional experimentation. This workflow is by no means an absolute, rigid path but rather a guide in how to efficiently produce to meaningful data to be assemble a preclinical package to move into human trials. Future directions for this workflow include new implementation and use to study additional rare and orphan diseases. Training new undergraduate researchers to continue this arm of research in the Gavegnano group is underway, as we hope the goals and aims for rare and orphan disease discovery continue far beyond this honors thesis.

References

- (1) *Rare Disease Day: Frequently Asked Questions*; NORD, 2019. <https://rarediseases.org/wp-content/uploads/2019/01/RDD-FAQ-2019.pdf>.
- (2) (FDA), F. a. D. A. *Rare Diseases at FDA*. 2022. <https://www.fda.gov/patients/rare-diseases-fda> (accessed 2023 02/22/2023).
- (3) Aartsma-Rus, A.; Dooms, M.; Le Cam, Y. Orphan Medicine Incentives: How to Address the Unmet Needs of Rare Disease Patients by Optimizing the European Orphan Medicinal Product Landscape Guiding Principles and Policy Proposals by the European Expert Group for Orphan Drug Incentives (OD Expert Group). *Frontiers in Pharmacology* **2021**, *12*, Policy and Practice Reviews. DOI: 10.3389/fphar.2021.744532.
- (4) Neha, D.; Ashish, J.; Dhruv, M.; Ajay, P.; Bikash, M. Drug Repurposing and Orphan Disease Therapeutics. In *Drug Repurposing*, Farid, A. B. Ed.; IntechOpen, 2020; p Ch. 4.
- (5) Muller, P. Y.; Milton, M. N. The determination and interpretation of the therapeutic index in drug development. *Nature Reviews Drug Discovery* **2012**, *11* (10), 751-761. DOI: 10.1038/nrd3801.
- (6) Taylor, J. P. Multisystem proteinopathy: Intersecting genetics in muscle, bone, and brain degeneration. *Neurology* **2015**, *85* (8), 658-660. DOI: 10.1212/WNL.0000000000001862.
- (7) Pfeffer, G.; Lee, G.; Pontifex, C. S.; Fanganiello, R. D.; Peck, A.; Weihl, C. C.; Kimonis, V. Multisystem Proteinopathy Due to VCP Mutations: A Review of Clinical Heterogeneity and Genetic Diagnosis. *Genes* **2022**, *13* (6), 963.
- (8) Korb, M. K.; Kimonis, V. E.; Mozaffar, T. Multisystem proteinopathy: Where myopathy and motor neuron disease converge. *Muscle & Nerve* **2021**, *63* (4), 442-454. DOI: <https://doi.org/10.1002/mus.27097>.
- (9) Kim, H. J.; Kim, N. C.; Wang, Y.-D.; Scarborough, E. A.; Moore, J.; Diaz, Z.; MacLea, K. S.; Freibaum, B.; Li, S.; Molliex, A.; et al. Mutations in prion-like domains in hnRNPA2B1 and hnRNPA1 cause multisystem proteinopathy and ALS. *Nature* **2013**, *495* (7442), 467-473. DOI: 10.1038/nature11922.
- (10) Korb, M.; Peck, A.; Alfano, L. N.; Berger, K. I.; James, M. K.; Ghoshal, N.; Healzer, E.; Henchcliffe, C.; Khan, S.; Mammen, P. P. A.; et al. Development of a standard of care for patients with valosin-containing protein associated multisystem proteinopathy. *Orphanet Journal of Rare Diseases* **2022**, *17* (1), 23. DOI: 10.1186/s13023-022-02172-5.
- (11) Mehta, S. G.; Khare, M.; Ramani, R.; Watts, G. D.; Simon, M.; Osann, K. E.; Donkervoort, S.; Dec, E.; Nalbandian, A.; Platt, J.; et al. Genotype-phenotype studies of VCP-associated inclusion body myopathy with Paget disease of bone and/or frontotemporal dementia. *Clin Genet* **2013**, *83* (5), 422-431. DOI: 10.1111/cge.12000 From NLM.
- (12) Pfeffer, G.; Lee, G.; Pontifex, C. S.; Fanganiello, R. D.; Peck, A.; Weihl, C. C.; Kimonis, V. Multisystem Proteinopathy Due to VCP Mutations: A Review of Clinical Heterogeneity and Genetic Diagnosis. *Genes (Basel)* **2022**, *13* (6). DOI: 10.3390/genes13060963 From NLM.
- (13) Meyer, H.; Weihl, C. C. The VCP/p97 system at a glance: connecting cellular function to disease pathogenesis. *Journal of Cell Science* **2014**, *127* (18), 3877-3883. DOI: 10.1242/jcs.093831 (accessed 3/13/2023).
- (14) Bayraktar, O.; Oral, O.; Kocaturk, N. M.; Akkoc, Y.; Eberhart, K.; Kosar, A.; Gozuacik, D. IBMPFD Disease-Causing Mutant VCP/p97 Proteins Are Targets of Autophagic-Lysosomal Degradation. *PLOS ONE* **2016**, *11* (10), e0164864. DOI: 10.1371/journal.pone.0164864.

- (15) Wani, A.; Weihl, C. C. Loss-of-function mutation in VCP mimics the characteristic pathology as in FTLT-TARDBP. *Autophagy* **2021**, *17* (12), 4502-4503. DOI: 10.1080/15548627.2021.1985880.
- (16) van den Boom, J.; Meyer, H. VCP/p97-Mediated Unfolding as a Principle in Protein Homeostasis and Signaling. *Molecular Cell* **2018**, *69* (2), 182-194. DOI: 10.1016/j.molcel.2017.10.028 (accessed 2023/03/14).
- (17) Tresse, E.; Salomons, F. A.; Vesa, J.; Bott, L. C.; Kimonis, V.; Yao, T.-P.; Dantuma, N. P.; Taylor, J. P. VCP/p97 is essential for maturation of ubiquitin-containing autophagosomes and this function is impaired by mutations that cause IBMPFD. *Autophagy* **2010**, *6* (2), 217-227. DOI: 10.4161/auto.6.2.11014.
- (18) Ferrari, V.; Cristofani, R.; Tedesco, B.; Crippa, V.; Chierichetti, M.; Casarotto, E.; Cozzi, M.; Mina, F.; Piccolella, M.; Galbiati, M.; et al. Valosin Containing Protein (VCP): A Multistep Regulator of Autophagy. *Int J Mol Sci* **2022**, *23* (4). DOI: 10.3390/ijms23041939 From NLM.
- (19) Kocaturk, N. M.; Gozuacik, D. Crosstalk Between Mammalian Autophagy and the Ubiquitin-Proteasome System. *Front Cell Dev Biol* **2018**, *6*, 128. DOI: 10.3389/fcell.2018.00128 From NLM.
- (20) Iwata, A.; Riley, B. E.; Johnston, J. A.; Kopito, R. R. HDAC6 and Microtubules Are Required for Autophagic Degradation of Aggregated Huntingtin*. *Journal of Biological Chemistry* **2005**, *280* (48), 40282-40292. DOI: <https://doi.org/10.1074/jbc.M508786200>.
- (21) Pandey, U. B.; Nie, Z.; Batlevi, Y.; McCray, B. A.; Ritson, G. P.; Nedelsky, N. B.; Schwartz, S. L.; DiProspero, N. A.; Knight, M. A.; Schuldiner, O.; et al. HDAC6 rescues neurodegeneration and provides an essential link between autophagy and the UPS. *Nature* **2007**, *447* (7146), 860-864. DOI: 10.1038/nature05853.
- (22) Pizzino, G.; Irrera, N.; Cucinotta, M.; Pallio, G.; Mannino, F.; Arcoraci, V.; Squadrito, F.; Altavilla, D.; Bitto, A. Oxidative Stress: Harms and Benefits for Human Health. *Oxid Med Cell Longev* **2017**, *2017*, 8416763. DOI: 10.1155/2017/8416763 From NLM.
- (23) Elbatreek, M. H.; Mucke, H.; Schmidt, H. H. H. W. NOX Inhibitors: From Bench to Naxibs to Bedside. In *Reactive Oxygen Species : Network Pharmacology and Therapeutic Applications*, Schmidt, H. H. H. W., Ghezzi, P., Cuadrado, A. Eds.; Springer International Publishing, 2021; pp 145-168.
- (24) Thannickal, V. J.; Jandeleit-Dahm, K.; Szyndralewicz, C.; Török, N. J. Pre-clinical evidence of a dual NADPH oxidase 1/4 inhibitor (setanaxib) in liver, kidney and lung fibrosis. *Journal of Cellular and Molecular Medicine* **2023**, *27* (4), 471-481. DOI: <https://doi.org/10.1111/jcmm.17649>.
- (25) Schildknecht, S.; Weber, A.; Gerding, H. R.; Pape, R.; Robotta, M.; Drescher, M.; Marquardt, A.; Daiber, A.; Ferger, B.; Leist, M. The NOX1/4 inhibitor GKT136901 as selective and direct scavenger of peroxynitrite. *Curr Med Chem* **2014**, *21* (3), 365-376. DOI: 10.2174/09298673113209990179 From NLM.
- (26) Cha, J. J.; Min, H. S.; Kim, K. T.; Kim, J. E.; Ghee, J. Y.; Kim, H. W.; Lee, J. E.; Han, J. Y.; Lee, G.; Ha, H. J.; et al. APX-115, a first-in-class pan-NADPH oxidase (Nox) inhibitor, protects db/db mice from renal injury. *Laboratory Investigation* **2017**, *97* (4), 419-431. DOI: 10.1038/labinvest.2017.2.
- (27) Trocoli, A.; Djavaheri-Mergny, M. The complex interplay between autophagy and NF- κ B signaling pathways in cancer cells. *Am J Cancer Res* **2011**, *1* (5), 629-649. From NLM.

- (28) Liu, C.; Arnold, R.; Henriques, G.; Djabali, K. Inhibition of JAK-STAT Signaling with Baricitinib Reduces Inflammation and Improves Cellular Homeostasis in Progeria Cells. *Cells* **2019**, *8* (10), 1276.
- (29) Dudley, A. C.; Thomas, D.; Best, J.; Jenkins, A. The STATs in cell stress-type responses. *Cell Commun Signal* **2004**, *2* (1), 8. DOI: 10.1186/1478-811x-2-8 From NLM.
- (30) Aydoğdu, N.; Öztel, O. N.; Karaöz, E. Isolation, Culture, Cryopreservation, and Preparation of Skin-Derived Fibroblasts as a Final Cellular Product Under Good Manufacturing Practice–Compliant Conditions. In *Stem Cells and Good Manufacturing Practices: Methods, Protocols, and Regulations*, Turksen, K. Ed.; Springer US, 2021; pp 85-94.
- (31) M. Reece, N. B., L. Ramirez, C. Gavegnano, B. Kim Rufinamide-induced autophagy cell death in HIV-1-infected macrophages. In AIDS2022, 2022.
- (32) Nalbandian, A.; Llewellyn, K. J.; Nguyen, C.; Yazdi, P. G.; Kimonis, V. E. Rapamycin and chloroquine: the in vitro and in vivo effects of autophagy-modifying drugs show promising results in valosin containing protein multisystem proteinopathy. *PLoS One* **2015**, *10* (4), e0122888. DOI: 10.1371/journal.pone.0122888 From NLM.
- (33) Lin, X.; Han, L.; Weng, J.; Wang, K.; Chen, T. Rapamycin inhibits proliferation and induces autophagy in human neuroblastoma cells. *Biosci Rep* **2018**, *38* (6). DOI: 10.1042/bsr20181822 From NLM.